Diamond & Related Materials 68 (2016) 1–9

Contents lists available at ScienceDirect

Diamond & Related Materials

journal homepage: www.elsevier.com/locate/diamond

Synergistic effect of Cu/Cr co-doping on the wettability and mechanical properties of diamond-like carbon films

Lili Sun [a,b], Peng Guo [a], Peiling Ke [a], Xiaowei Li [a,*], Aiying Wang [a,*]

[a] Key Laboratory of Marine Materials and Related Technologies, Zhejiang Key Laboratory of Marine Materials and Protective Technologies, Ningbo Institute of Materials Technology and Engineering, Chinese Academy of Sciences, Ningbo 315201, PR. China
[b] University of Chinese Academy of Sciences, Beijing 100049, PR. China

ARTICLE INFO

Article history:
Received 8 April 2016
Received in revised form 10 May 2016
Accepted 20 May 2016
Available online 24 May 2016

Keywords:
Co-doping
Synergistic effect
Wettability
Surface energy
Diamond-like carbon

ABSTRACT

By choosing carbide-forming element Cr and non-carbide-forming element Cu as co-doped metal elements, we firstly fabricated Cu and Cr co-doped diamond-like carbon (Cu/Cr-DLC) films using a facile hybrid ion beam deposition system. The effect of Cu/Cr co-doping on wettability and mechanical properties of DLC films were focused. The resultant Cu/Cr-DLC films were shown to afford good hydrophobicity and superior mechanical performance. In particular, the film with $Cu_{11.88\%}Cr_{6.57\%}$ (at.%) exhibited a relatively high water contact angle of 103.6°, lower residual stress of 0.89 GPa and high hardness of 13.44 GPa. The combined structural analysis demonstrated that the synergistic Cu/Cr co-doping resulted in the critical and significant relaxation of distorted C—C bond length, which ultimately caused the reduction in residual stress. Due to the formation of hard Cr carbide nano-particles in amorphous carbon matrix, the films maintained the high value of hardness. In addition, noted that the interesting wetting variety from hydrophilic to hydrophobic state was attributed to the enhanced surface graphitization and emergence of copper oxidation phases, and the film topographical microstructure could also promote the hydrophobicity of film when the maximum height of roughness was in a certain range. These results provide an expected robust synthesis method to make DLC film a promising protective coating for long lasting hydrophobic application and related harsh fields.

1. Introduction

Wettability of solid is a very important surface characteristic influencing a large range of material applications [1–2], such as anti-fogging [3], water-oil separation [4], self-cleaning [5] as well as drag reduction [6]. Amount of experimental results and theoretical calculations have confirmed that the wettability of solid surface depend on the surface free energy and the geometrical structure to a great extent [7–8]. However, if one keeps in mind the long lifetime durability and versatile low cost techniques, to develop the materials with low surface free energy together with excellent mechanical performance are still remaining the great challenge till now [9–10]. In particularly, when the mechanical components are exposed to the harsh conditions such as corrosion seawater, grave sand, and high moving speed etc. for related marine applications, the materials suffering from the serious corrosion and wear problems are required high hardness and good hydrophobicity.

Diamond-like carbon (DLC) films are one of the most promising candidates for the wide range of applications due to their extreme hardness, low friction, superior biocompatibility and chemical stability. However, the high compressive stress, poor adhesion to particular metal substrates and hydrophilic surface of DLC films are the key obstacles for their usage. Combined with hydrophobic wettability properties, DLC films have showed great possibility in applications of bio-robot, bio-medical devices and wear protection of MEMS surfaces [1,11–14]. Many efforts have been devoted so far to reduce compressive stress and improve the hydrophobicity of DLC films, wherein doping transition metal atoms into the amorphous carbon matrix is considered as an effective way to achieve the combined high performance by taking full advantage of the formed nanoparticulates of metal or metal carbides [15–16]. For instance, elements like Fe, Ni, Cu, Ti and Cr have been used to directly control the wettability as well as the mechanical properties of DLC films [17–21]. For a non-carbide-forming element, Cu doping led to the increase of water contact angle in DLC films. The hydrophobic feature attributed to the formed Cu nanoparticles, which had no advantage to generate dipole or saturate dangling bonds [19,21]. But both the stress and hardness of the film reduced drastically. On the other hand, adding carbide formed metal such as Cr or Ti into amorphous carbon matrix led to the stress reduction significantly without serious change of hardness, but decreased the water contact angle of film [20–21]. In view of the results described above, surface wetting behavior and mechanical property of DLC films shows distinct dependence upon the elemental features of doped metal. Especially, few efforts were devoted

* Corresponding authors.
E-mail addresses: lixw@nimte.ac.cn (X. Li), aywang@nimte.ac.cn (A. Wang).

http://dx.doi.org/10.1016/j.diamond.2016.05.006
0925-9635/

to developing the novel materials by taking the concept of synergistic effect from co-doped metals, in which both the residual stress and surface wettability could be optimized simultaneously according to the various demands of applications.

Based on our previous simulation results [22], where most of important result was that the anti-bonding feature of Cu element and nonbonding Cr element were selected to be co-doped into amorphous carbon matrix to reduce residual stress, we firstly brought forward the concept of Cu/Cr co-doped DLC films which could improve the mechanical properties and lower residual compressive stress of DLC films obviously by Cu/Cr co-doping. So in this work, the Cu/Cr co-doped DLC films were deposited by a hybrid ion beam system. The co-doped Cu/Cr concentration in DLC films was controlled by varying the sputtering current from 1.5 to 2.5 A. The effect of co-dopants on the surface wettability and mechanical properties of DLC films was investigated. In particular, the mechanism of wetting behavior was intensively discussed in terms of the surface energy and atomic bond structure of deposited films.

2. Experimental

2.1. Sample fabrication

Cu/Cr-DLC films were deposited on Si (P ⟨100⟩, 0.0015 Ω·cm) substrates by a hybrid ion beam deposition system [20], which combined an anode-layer ion beam source (LIS) and a rectangular DC magnetron sputtering with a composite Cu/Cr target (Jiangxi Ketai advanced material CO., LTD., 3N) at 1:1 atomic ratio. The LIS source enabled the facile deposition of DLC films by decomposing the hydrocarbon gas of C_2H_2, while the sputtering source benefited the versatile deposition of Cu/Cr co-doping by introducing Ar gas. Prior to deposition, the substrates were cleaned ultrasonically in acetone and ethanol for 15 min separately. After that, the substrates were located in the substrate holder with a distance about 15 cm from the center between metal target source and ion source. A base pressure of deposition chamber was about 2.7×10^{-3} Pa. In order to remove the surface adhered impurities, the substrates were thereafter cleaned by Ar ions for 10 min (etching thickness was about 115.5 nm). During deposition, the films were prepared for 15 min in the mixture precursors with 15 sccm C_2H_2 gas and 65 sccm Ar gas. In order to introduce the metal elements in carbon matrix without destroying the nature of amorphous carbon matrix, we in particular focused the metal doping on the small amount of metal concentration in the present work. Therefore, the Cu/Cr concentration was controlled by varying the sputtering current in a range of 1.5–2.5 A. The typical current of the LIS source and working pressure were 0.2 A and 0.6 Pa, respectively, and the power of the LIS source was 260 W, while that of sputtering source was in range of 1300–1500 W which varied with different sputtering currents. Meanwhile, a pulsed negative bias voltage of −100 V with 350 kHz was applied to the substrates during both the etching and deposition process.

2.2. Characterization

Thickness of the films was measured by a surface profilometer (Alpha-Step IQ) employing a step made by a shadow mask. The surface microstructure and Cu/Cr concentration of the films were analyzed comprehensively by field emission scanning electron microscopy (SEM) equipping with an energy dispersive X-ray spectroscopy (EDS, Hitachi S-4800). The surface morphology of films in a size of 3 μm × 3 μm was observed using a Scanning Probe Microscope (Dimension 3100 V, Veeco, US), and the atomic force microscopy (AFM) analyses were performed on a tapping mode, where the image analysis was carried out using a Nanoscope version 7.20 software. Raman spectroscopy (inVia-reflex, Renishaw) with 532 nm excitation wave length was employed to evaluate the carbon atomic bonds of films. Furthermore, the chemical composition and bonds of the films were characterized by X-ray photoelectron spectroscopy (XPS, ESCALAB 250, Thermo) with Al (mono) Kα irradiation. In order to get the accurate information of the surface, the measurement was taken directly without Ar^+ etching after taking from the chamber. High-resolution transmission electron microscope (HRTEM) of the DLC films was performed using a Tecnai F20 electron microscope (FEI company, Netherlands), which was operated at 200 keV with a pointed-to-point resolution of 0.24 nm. Mechanical properties were measured by the nano-indentation technique in a continuous stiffness measurement (CSM) mode with a maximum indentation depth of 300 nm. Six replicate indentations were made for each sample. The residual stress of the films was calculated from the curvature of the film/substrate was measured by a stress tester using a laser reflection method.

2.3. Wettability measurement and surface energy calculation

Static contact angle measurements were carried out by an OCA20 optical system (Dataphysics Ltd., Germany), 2 μl droplets of de-ionized water and glycerol (GI) were used as the working liquids in atmosphere at room temperature, respectively. The test was operated at five different regions on each sample. Generally, the surface energy of liquid or solid phase can be expressed by the addition of dispersion component and polar component, and the surface energy together with its polar and dispersive components can be finally quantified by the two liquids' components according to Fowkes model [23] and Owens-Wendt-Kaelble (OWK) model [24], the details about the mechanisms of the

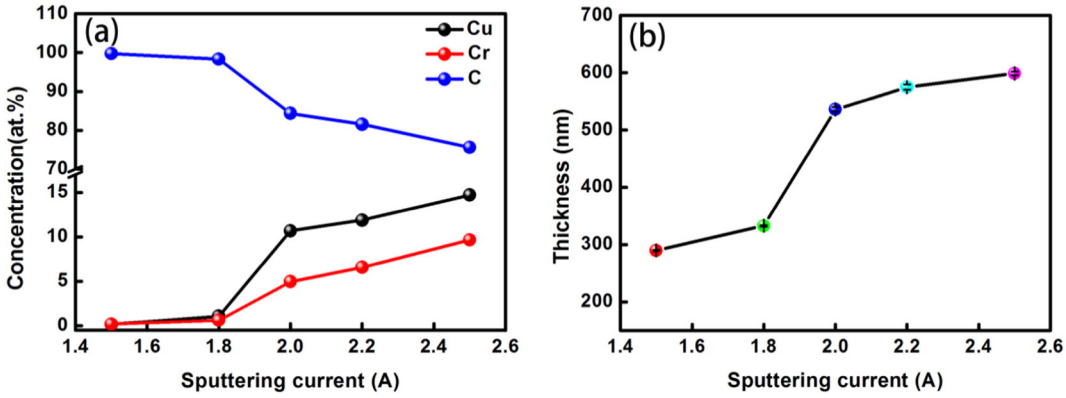

Fig. 1. (a) Composition and (b) thickness of the films as a function of sputtering current.

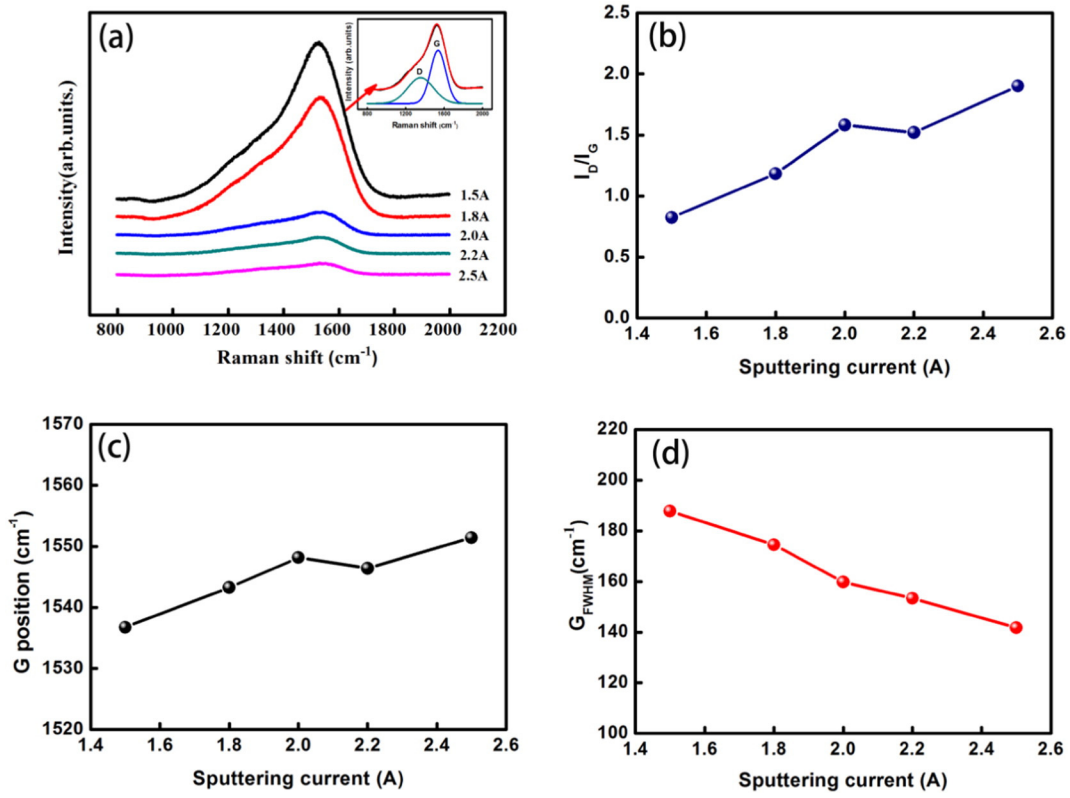

Fig. 2. (a) Raman spectra and typical deconvoluted Raman spectra of Cu/Cr-DLC films, (b) I_D/I_G , (c) G peak position and (d)the FWHM of G peak (G_{FWHM}) from Raman spectra as a function of sputtering current.

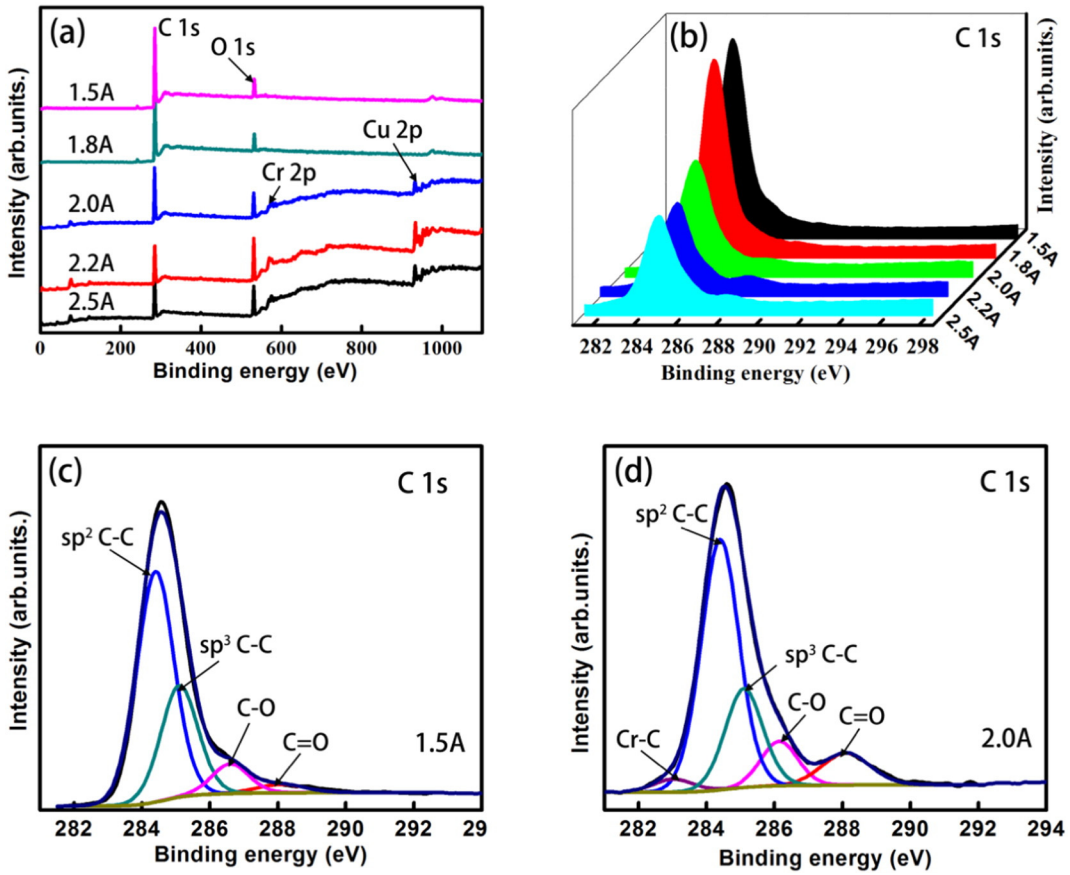

Fig. 3. (a) A survey XPS spectrum of Cu/Cr-DLC films, (b) C1s high resolution XPS spectra of Cu/Cr-DLC films, (c) and (d) Deconvoluted C 1s XPS spectra of the films deposited at 1.5 A and 2.2 A.

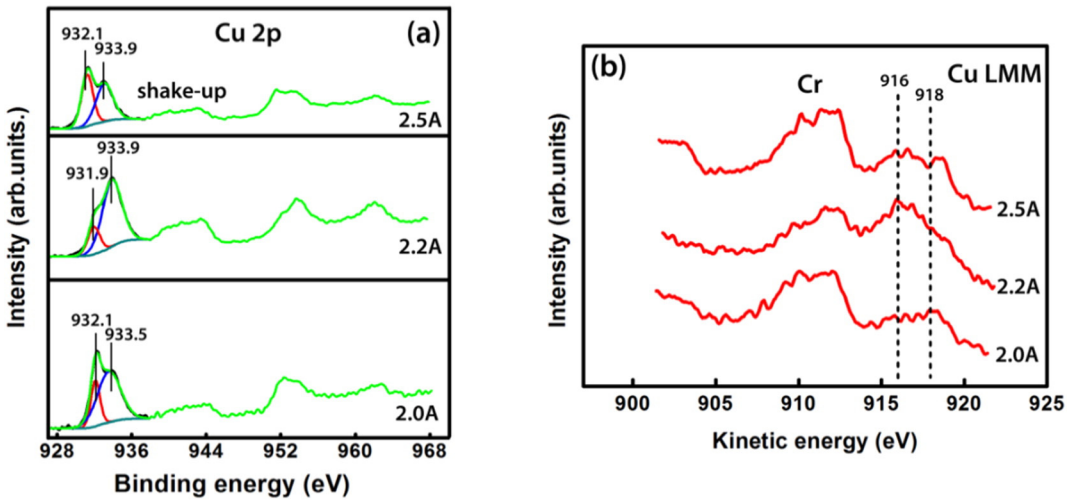

Fig. 4. (a) Main and satellite peak of Cu 2p of the XPS spectra and decomposing of Cu 2p3/2 main peak of 2.0–2.5 A, (b) Cu LMM Auger spectra for the surface examined by XPS.

OWK theory shows in the relevant reference [25], and the expression was as following:

$$1 + \cos\theta = 2\sqrt{\gamma_s^d}\left(\frac{\sqrt{\gamma_l^d}}{\gamma_l}\right) + 2\sqrt{\gamma_s^p}\left(\frac{\sqrt{\gamma_l^p}}{\gamma_l}\right) \quad (1)$$

where γ_l^d and γ_l^p are the dispersive and polar components of the surface free energy of the liquid, γ_s^d and γ_s^p are the corresponding dispersive and polar components of the surface free energy of the solid, respectively. Thus, a set of equations for two liquids with known polar and dispersive components (de-ionized water with $\gamma^p = 51.0$ mJ/m^2; $\gamma^d = 21.8$ mJ/m^2 and glycerol with $\gamma^p = 30.0$ mJ/m^2; $\gamma^d = 34.0$ mJ/m^2) can be solved [26].

3. Results and discussion

3.1. Deposition thickness and film composition

For easy description of composition script for Cu/Cr concentration, we thereafter employed the sputtering current as the dopant factor to investigate the effect of Cu/Cr co-doping on the microstructure and properties of DLC films. Fig. 1 shows the composition and thickness of deposited films with various sputtering currents. When the sputtering current increased from 1.5 to 2.5 A, both the Cu and Cr concentrations in the films increased monotonically and the C concentration decreased in the opposite tendency from 99.7 to 75.63 at.%, as shown in Fig. 1a. This demonstrated that the Cu/Cr co-doping with low concentration in DLC matrix was achieved by this versatile and facile hybrid ion beam technique. Nevertheless, noted that the doped Cu concentration (0.13–14.72 at.%) was much higher than that of Cr (0.17–9.65 at.%) within the sputtering current of 1.5–2.5 A. This attributed to the higher sputtering yield of non-carbide-forming Cu atom, which was about 1.12 for Cu and 0.5 for Cr [27]. Due to the increase of co-doped Cu/Cr contents in amorphous hydrogenated carbon matrix, as shown in Fig. 1b, the film thickness with sputtering current increased from 290 to 599 nm, corresponding to the average growth rate from 19.3 to 40 nm/min.

3.2. Film structure and atomic bond characteristic

As a standard non-destructive technique, Raman spectroscopy was used to record the changes in film microstructures. Fig. 2 shows the atomic bond structure of Cu/Cr-DLC films by Raman analysis. For all the samples, a broad asymmetric Raman scattering band was observed in the range of 1000–1700 cm^{-1}, demonstrating the typical characteristic of DLC film, as shown in Fig. 2a. However, noted that the peak intensity in the spectra decreased as the current increased from 1.5 to 2.5 A. This attributed to the increase of co-doped Cu and Cr concentrations with increasing sputtering current, which conduced to the carbon fraction decrease in per unit area to the Raman scattering and the decrease of spectra intensity. Generally, the Raman spectrum of DLC films can be decomposed by two-curve Gaussian function into two peaks (insert of Fig. 2a): D and G, where the D peak is attributed to the breathing mode of sp^2 atoms in rings at around 1350 cm^{-1} and G peak is related

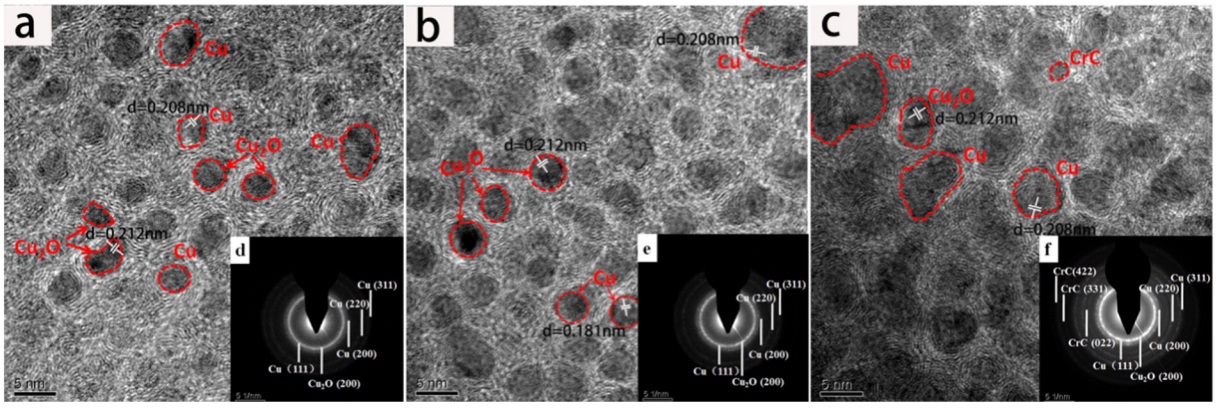

Fig. 5. HRTEM bright-field images and corresponding diffraction pattern of the Cu/Cr-DLC films: (a) and (d) 1.5 A, (b) and (e) 2.0 A, and (c) and (f) 2.2 A.

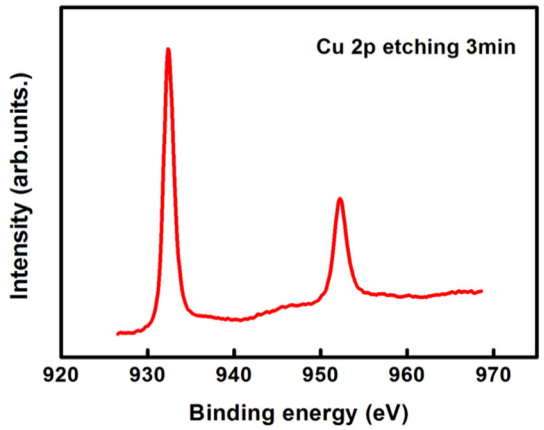

Fig. 6. XPS Cu 2p of film at the current of 2.2 A after Ar+ etching 3 min.

to the stretching mode of all pairs of sp^2 carbon atoms in both rings and chains located at around 1580 cm^{-1} [28]. According to the intensity ratio of D peak to G peak (I_D/I_G), G peak position, and full width at half maximum of G peak (G_{FWHM}), the atomic bond of DLC films can be deduced. When sputtering current increased from 1.5 to 2.5 A, I_D/I_G ratio increased monotonically from 0.82 to 1.9, the G peak position shifted upward from 1536.75 to 1551.43 cm^{-1} and G_{FWHM} decreased monotonically from 187.82 to 147.15 cm^{-1} (Fig. 2b–d), this behavior indicated the increase in the size and number of the sp^2 clusters in Cu/Cr-DLC films. Furthermore, since the G_{FWHM} is mainly sensitive to the structural disorder arising from the bond angle and bond length distortions in the film, it could be concluded that the incorporation of Cu/Cr caused structural ordering and promoted the formation of C═C bonds organized in delocalized rings. In brief, the results obtained from G peak position, I_D/I_G ratio and G_{FWHM} value clearly revealed an enhancement in graphite-like character with Cu/Cr co-doping and the film at 2.5 A exhibited the high degree of graphite-like character (sp^2 bonding) and highest value of sp^2 carbon clustering.

The XPS analysis was employed to investigate the elemental bonding states in Cu/Cr-DLC films. Fig. 3a shows the full-range XPS spectra of films with various sputtering currents. C 1s, O 1s, Cr 2p and Cu 2p were observed for the 2.0, 2.2 and 2.5 A, whereas no obvious distinct Cr 2p and Cu 2p signal was detected for 1.5 and 1.8 A. Meanwhile, there was some oxygen in the films as a result of contamination from the residual vacuum. Thus, the XPS signal information revealed that the Cu/Cr metals were successfully doped into the DLC matrix, where the amount of Cu/Cr doping was found to increase with the increasing sputtering current. To further understand the bonding state of carbon in films, C 1s spectra were investigated in depth using high-resolution XPS, as can be seen in Fig. 3b. The XPS C1s spectra contained a large asymmetric peak suggesting the existence of carbon atoms in various bonding states (Fig. 3b). At the current of 1.5 A, the C 1s spectrum was deconvoluted, and four peaks were obtained. The four peaks corresponded to the sp^2-C group around 284 eV, the sp^3-C group around 285 eV, the C—O group around 286 eV and the C═O group around 288 eV [20]. More importantly, the chromium carbide peak with a binding energy around 283 eV was invisible due to a low doped Cr concentration, which agreed well with the previous results [29,30]. For the case of current at 2.2 A, a peak with 283 eV for Cr—C bond was obtained in the spectra, except the fitted four peaks with binding energies at 284 eV for sp^2 bonds, 285 eV for sp^3 bonds, 286 eV for C—O bonds, 288 eV for C═O bonds. This showed that the chromium carbide emerged in the film due to the higher Cr doped concentration and the chemical reaction between C and Cr atoms [31].

To elucidate the chemical state of Cu dopant in the films, moreover, we investigated the main and the satellite peaks of Cu $2p_{3/2}$ and Cu $2p_{1/2}$ XPS spectra for the deposited films, as shown in Fig. 4a. When the current was less than 1.8 A, no peak was displayed in spectra owning to the low Cu/Cr concentration. Beyond of current 2.0 A, the satellite feature peaks (938–945 eV) were evident from the spectra. Considering the characteristic peak of CuO is a shake-up satellite peak which always accompanied with the main peak at about 9 eV higher binding energy position [32], it could be concluded that the CuO phase formed in these films. On the other hand, a split shoulder peak with main peak of Cu $2p_{3/2}$ implied the possibility of other phases including CuO one. The main peak Cu $2p_{3/2}$ of films were decomposed into two peaks around 932 eV and 934 eV relating to Cu_2O or Cu and CuO respectively, which confirmed the existing of different copper phases. Unfortunately, Cu and Cu_2O phases cannot be distinguished by this decomposing because their binding energies were very close. To definite the unknown phases, fine informative analysis about LMM Auger transition in XPS spectra for Cu and Cu_2O was carried out to avoid the divergence from the decomposed binding energy [33]. As shown in Fig. 4b, the Cu LMM Auger spectra were reflected in a broad peak from 915 eV to 920 eV appearing in the spectra, in which the peak around 916 eV confirmed the assumption of formed Cu_2O phase, while the peak around 918 eV indicated the possibility of Cu and CuO phases [34]. At the current of 2.0 A, no obvious peak of Cu_2O phase was observed, but the intensity of Cu_2O

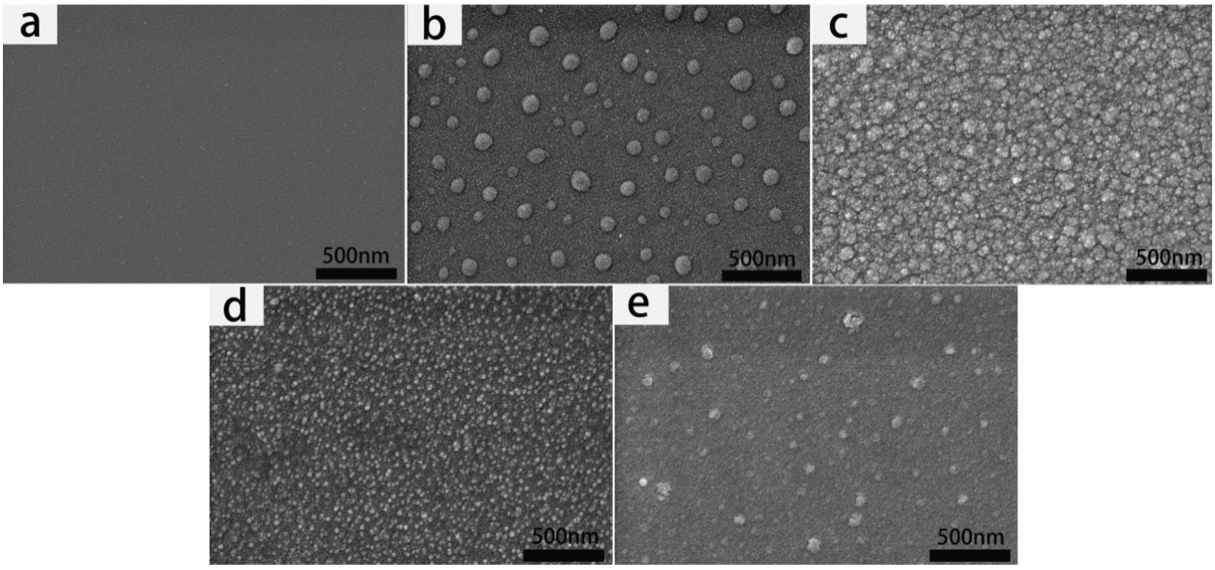

Fig. 7. SEM image of Cu/Cr-DLC films with different sputtering current: (a) 1.5 A, (b) 1.8 A, (c) 2.0 A, (d) 2.2 A, (e) 2.5 A.

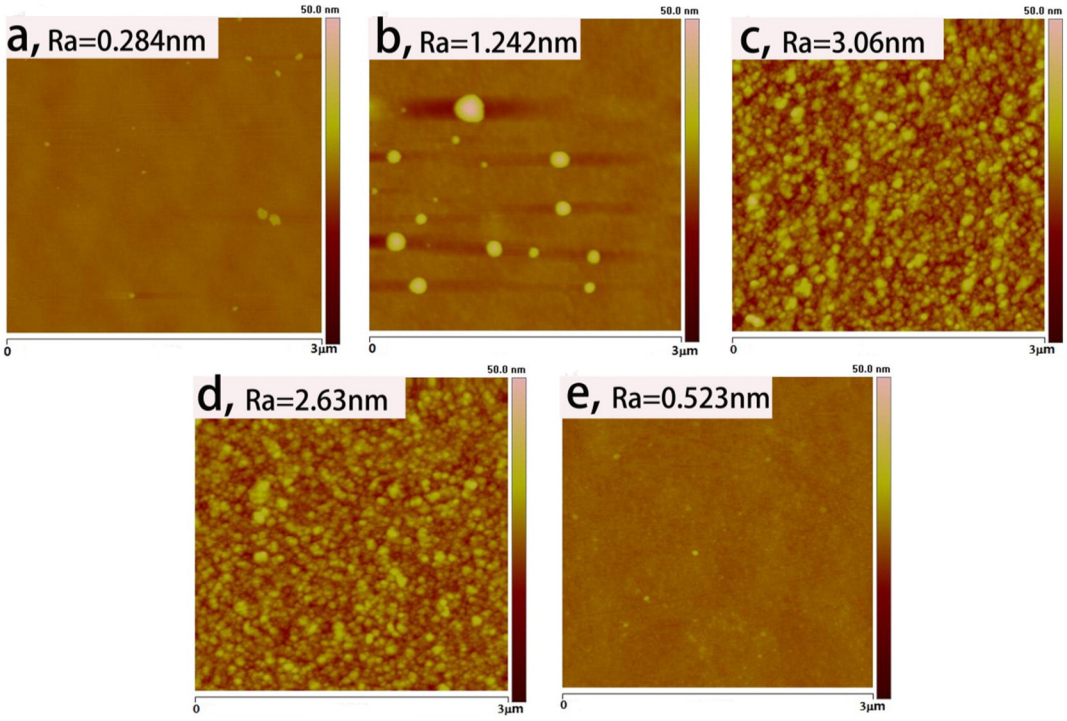

Fig. 8. AFM images of Cu/Cr-DLC films deposited at (a) 1.5 A, (b) 1.8 A, (c) 2.0 A, (d) 2.2 A, (e) 2.5 A.

peak enhanced with the current. It could thus be said that the obvious copper oxidation on the surface enhanced with the Cu/Cr concentration.

In order to gain insight into the microstructure evolution of films, high resolution TEM was observed as Fig. 5, which showed the TEM images and selected diffraction pattern for the films deposited at current of 1.5, 2.0 and 2.2 A, respectively. Obviously, all the films illustrated the nanocomposite structure where the nanoparticulates were embedded uniformly into the amorphous DLC matrix. In the case of current at 1.5 and 2.0 A, the nanoparticulates were designed to the Cu and Cu_2O clusters, while the signal of doped Cr atoms could not be recognized because of a high solid solubility of Cr atoms in carbon matrix [19,29] and the difference bonding feature of Cr—C and Cu—C [22]. When the current was 2.2 A, the intensity of diffraction selected pattern increased significantly. More detail structure of the nanoparticulates could be identified according to the mutual lattice spacing. In contrast to the cases at 1.5 and 2.0 A, the chromium carbide phase emerged at 2.2 A, which agreed well with the combined XPS analysis above. Meanwhile, Fig. 5 also reveals that the amorphous carbon matrix consisted of some nanoclusters and curved planes forming onion-like structures, indicating that Cr could crosslink and bend the graphite planes as explained by other authors [35–36]. But it should be mentioned that there were no obviously CuO phase in all these films, because the CuO phase was an unstable material which was easy to generate stable Cu_2O during the process of TEM sample preparing. Balamurugan et al. [37] also mentioned that the more symmetric cubic Cu_2O phase should be more stable than the monoclinic CuO phase at smaller size. On the other hand, this indirectly indicated that there was just a very thin CuO layer on Cu or Cu_2O nanoparticulates. Based on this assumption, we observed the Cu 2p XPS of 2.2 A with 3 min Ar^+ etching (Fig. 6). The satellite peak accompanied with the main peak was absent after surface etching, which meant the CuO phase just emerged with a very thin layer on the shallow surface.

3.3. Morphological analysis

The surface morphology of the samples obtained at different sputtering current was characterized by SEM technique. The SEM micrographs showed in Fig. 7 illustrate the significant changes in surface morphology. When the current was 1.5 A, the film showed a typical smooth surface similar to that of pure DLC films. In case of current at 1.8 A, some nanosphere particulates with diameter of 60–120 nm appeared in the film surface, as illustrated in Fig. 7b. Further increasing the current to 2.0 A resulted in the cauliflower-like morphology, where the denser and compact nanoparticulates were visible. However, it was of interest that the cauliflower-like topology disappeared as the current increased to 2.2 A, and the surface became to be smoother. For the case of 2.5 A current, the small nanosphere particles started to be involved again in the surface. Two reasons could be employed to understand this evolution of surface morphology. First, the different solid solubility of doped metal atoms in carbon matrix and the lowered ion mobility in the growing surface resulted from the Cu/Cr concentration [21]. For instance, if the solid solubility of doped metal element in DLC matrix was approximately designated by the threshold value of metal concentration, the doped metal atoms started to precipitate in nanoparticulates from the amorphous carbon matrix. The solid solubility of doped Cu was about 1.93 at.% while it was about 8.42 at.% for Cr in our previous work [19,29]. Second, it was worth noticing that, the monometal doped DLC films like Cu-DLC or Cr-DLC, the size of formed Cu

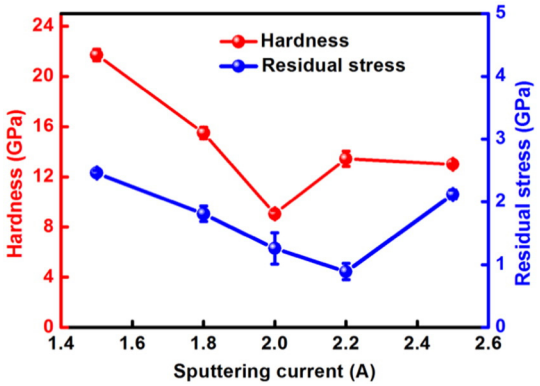

Fig. 9. Hardness and residual stress curves for films at different sputtering current.

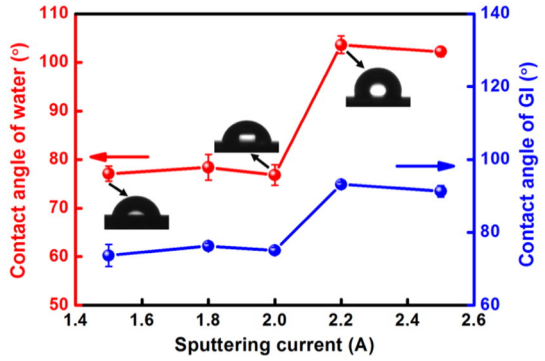

Fig. 10. De-ionized water and GI contact angles of the Cu/Cr-DLC films with different sputtering currents.

nanoparticulates or chromium carbide ones increased monotonically with Cu or Cr concentration [19,29]. As a result, the synergistic competition between Cu and Cr doped atoms enabled the dramatic evolution of surface morphology during film growth.

The average roughness Ra of the obtained films was showed in Fig. 8 by AFM technique. Within the small scanning area of 3 μm × 3 μm, all the film surfaces were relatively smooth but had the arithmetic average roughness less than 3.2 nm, the surfaces did not show a monotonic trend in roughness of these nano-structured DLC films. The topography analysis indicated the nanosphere particulates appeared in the case of current at 1.8 A and they became denser and refinement till the current increased to 2.2 A. In case of current at 2.5 A, the film recovered a smooth surface. This result was consistent with the analysis of measured SEM morphology, which meant all the films had a grainy surface with average grain size increasing first and then decreasing with deposition sputtering current, Nevertheless, Ra had not large deviations, varying in the range of 0.284–3.06 nm.

3.4. Residual stress and mechanical properties

Fig. 9 shows the dependence of the residual compressive stress and hardness in the film on the sputtering current. In the initial stage, it was clear that there was a decrease in the residual stress, in which the sputtering current increased from 1.5 to 2.2 A, the stress decreased monotonically from 2.46 ± 0.04 to 0.89 ± 0.13 GPa. When sputtering current increased to 2.5 A, the residual stress significantly increased to 2.12 ± 0.07 GPa, Li et al. [22] suggested that a small amount of Cu and Cr doped into amorphous carbon matrix would result in the critical and significant relaxation of distorted C—C bond lengths. On the other hand, a weak bonding interaction between the Cr and C atoms, and the antibonding interaction observed for the Cu—C bonds, would play a pivot site for the release of strain energy [38]. At the same time, the increase of the sp^2 content from the Raman analysis, as the other important factor, would cause the decrease of the internal stress. As a result, the two potent factors finally led to a relatively stable value of 0.89 ± 0.13 GPa at 2.2 A. However, as doping of more Cu/Cr atoms, on one hand, more Cr carbides were formed. Since the Cr—C bond length is longer than the C—C bond length [39]. On the other hand, higher Cu concentration would result in the increase of distorted C—C bond lengths and the existence of distorted C—Cu structures [22]. Therefore, the residual stress increased rapidly.

The hardness showed a similar trend as that of residual stress, the difference was that the lowest hardness appeared at 2.0 A and then increased to 13.44 ± 0.61 GPa at 2.2 A, and finally it slightly decreased to 13 ± 0.07 GPa at 2.5 A (Fig. 9). Usually, it is well known that there is a close relationship between the hardness and the sp^2/sp^3 ratio. Combining the Raman and XPS analysis, the sp^2 content increased with the sputtering current, which contributed to the decreased hardness. Meanwhile, incorporated Cr atom in the film played a pivotal role. On the one hand, the hard Cr carbides could easily form, because of its bonding characteristics with the C atom. On the other hand, the formation of hard Cr carbide or metal nano-cluster phase could break the continuity of the carbon network, and result in the decrease in hardness [40]. There was a certain competition between the above mentioned two processes. At the beginning, with the sputtering current from 1.5 to 2.0 A, no metal carbide formed, the Cr crosslinked and bent the graphite planes, and soft Cu metal cluster embedded in the carbon network, which would decrease the hardness of the films. However, as the Cr content increased (beyond of 2.2 A), a large amount of Cr carbides formed and enhanced the hardness. Further, the amount of soft Cu metal and its oxidation cluster increased because of high Cu sputtering yield, and finally caused the hardness to slightly decrease at 2.5 A.

3.5. Wetting behavior

Fig. 10 illustrates the obvious wettability transformation from hydrophilic state to hydrophobic state as the current increased from 1.5 to 2.5 A. Specifically, when the current was less than 2.0 A, the films were hydrophilic and the water contact angle (WCA) was kept around 77.11 + 1.52°. However, the films became to be hydrophobic when the current further reached up to 2.2 A and 2.5 A, respectively, where the WCA was maintained around 103.6 ± 1.82°. The GI contact angle for the films with the sputtering current showed a similar trend, increasing from 73.7 ± 3° to 93.2 ± 0.63°.

In order to exploit the mechanism of wettability transformation of Cu/Cr-DLC films, the surface energy of films was surveyed. Fig. 11a shows the total surface energy which could be divided into the dispersive and polar components of the films determined by the employed two liquids. Similar to the tendency of contact angle, two different states were observed in the evolution of surface energy with the sputtering current. When the sputtering current increased from 1.5 to 2.0 A, the

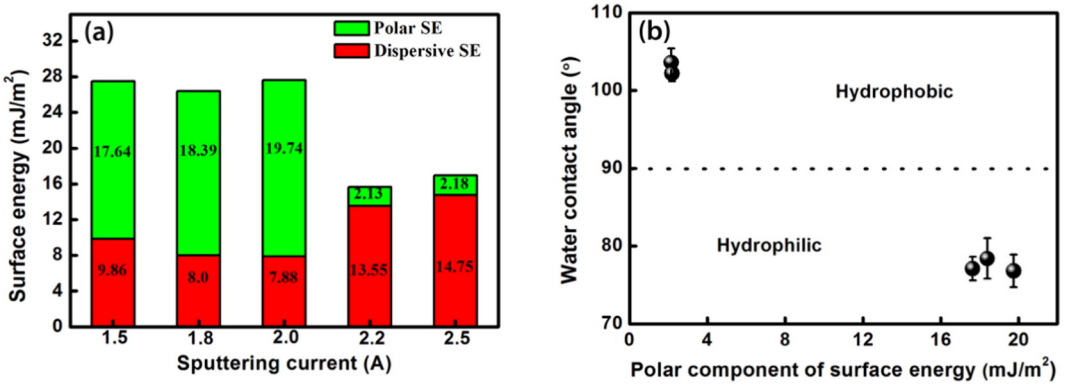

Fig. 11. (a) Polar and dispersive component of surface energies of Cu/Cr-DLC films, (b) Variation of water contact angles of Cu/Cr-DLC films with polar component of their surface energies.

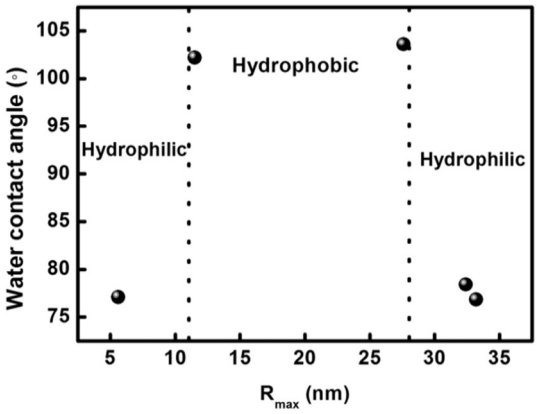

Fig. 12. Variation of water contact angles of Cu/Cr-DLC films with R_{max}.

total surface energy and the polar component of the films had no obvious change, which were maintained around 27.17 ± 0.78 and 18.59 ± 1.15 mJ/m^2, respectively. However, further increasing the current to 2.2 and 2.5 A led to the significant decrease of the total surface energy and the polar component which were 14.15 ± 0.6 and 2.155 ± 0.025 mJ/m^2, respectively. More clear dependence of polar component in surface energy on the WCA for the films was elucidated in Fig. 11b. When the polar component of surface energy was less than 2.2 mJ/m^2, the films were hydrophobic. However, the films transferred to be hydrophilic as the polar component was beyond of 17.5 mJ/m^2, in which the current was in the range of 1.5–2.0 A. In general, the electric dipole of water molecule was attracted usually by the polar component of solid surface [41]. The interfacial energy between the film surface and water increased with the reduction of polar component, and as a consequence the WCA increased. In this case, it could be said reasonably that, the change in polar component of the surface energy might be the dominated factor for the variety of surface wettability in Cu/Cr-DLC films.

According to the in-depth analysis of film chemical structure, the formation of promoted sp^2 carbon and the emergence of copper oxidation could be the main reasons for reduction of the surface energy and its polar part. Firstly, the wettability of DLC film was closely related to the sp^2/sp^3 ratio on the surface [42], the sp^2-rich surface would decrease the polar component in surface energy by decreasing the dangling bonds and therefore resulted in the hydrophobicity [43–44]. Regarding the combined analysis of WCA and surface energy above, the increased sp^2 bonds in the Cu/Cr-DLC films might result in the increase of WCA. Secondly, from Fig. 4, it is obvious that, as beyond of 2.0 A, the copper oxidation on the surface increased with the sputtering current. One knows that the weaker the electronegativity, the lower the polar component of the surface energy. Regarding the electronegativity of these compounds obeyed as follows: Cu > CuO > Cu_2O [45], it could thus be said that the obvious copper oxidation played an important role in lowering the polar component of the surface energy.

Besides these, topographical microstructure is another factor governed the wettability of films [46]. Although there was small variation in average roughness Ra among these films (Fig. 8), surface topography was inherently three dimensional, the impact of nanosphere particulates of different Cu/Cr-DLC films could never be neglected. Therefore, using only R_a value as a roughness indicator could not reflect the characteristics of the surface accurately. Owning to the close relationship between the nanoparticles and maximum height of roughness (R_{max}), the described diagram between WCA and R_{max} is presented as Fig. 12. The wettability of Cu/Cr-DLC films showed hydrophobic state when R_{max} located at the range of 11.5–27.6 nm, but when the value of R_{max} was beyond this range, the films kept the hydrophilic state. As we know that the value of R_{max} is dominated by the feature of the nano-particles in the film, it indicated that the size of these nanosphere particulates in Cu/Cr-DLC film could affect the wettability state of films.

As the results above, we concluded the intrinsic water wettability of Cu/Cr-DLC films as Fig. 13. With low concentration of Cu/Cr doping, the surface of the film was composed of small amount of doped metal atoms, low ratio of sp^2 C—C to sp^3 C—C, which contained a large amount of dangling bonds to attract the water molecule in atmosphere. With the increase of Cu/Cr doping and the synergistic effect, the improved sp^2-rich surface led to the decrease of dangling bonds; moreover, the oxidation of Cu exposed in the surface further weakened the interaction between the film and the water molecules. Combining with the surface topographical microstructure, the film showed a hydrophobic state at high concentration of Cu/Cr co-doping. In view of the results described above, increasing the size and quantity of Cu and Cu oxidation particles in Cu/Cr-DLC film could further improve the hydrophobicity of film.

4. Conclusion

In summary, we firstly brought forward the design of novel Cu/Cr co-doped amorphous carbon films by a hybrid ion beam deposition system. The Cu/Cr concentration in the films could be altered from $Cu_{0.13}Cr_{0.17}$ (at.%) to $Cu_{14.72}Cr_{9.65}$ (at.%) by varying the sputtering current from 1.5 to 2.5 A systemically. The results revealed that the synergistic Cu/Cr co-doping in DLC matrix caused the wettability transforming from hydrophilic to hydrophobic state. In particular, increasing the co-doped Cu/Cr concentration led to a lower residual stress and high hardness. Results indicated that the increase of graphitization of films and oxidation of copper, decreased the total surface energy and the polar component, the addition of Cu and Cr impurities in DLC resulted in the critical and

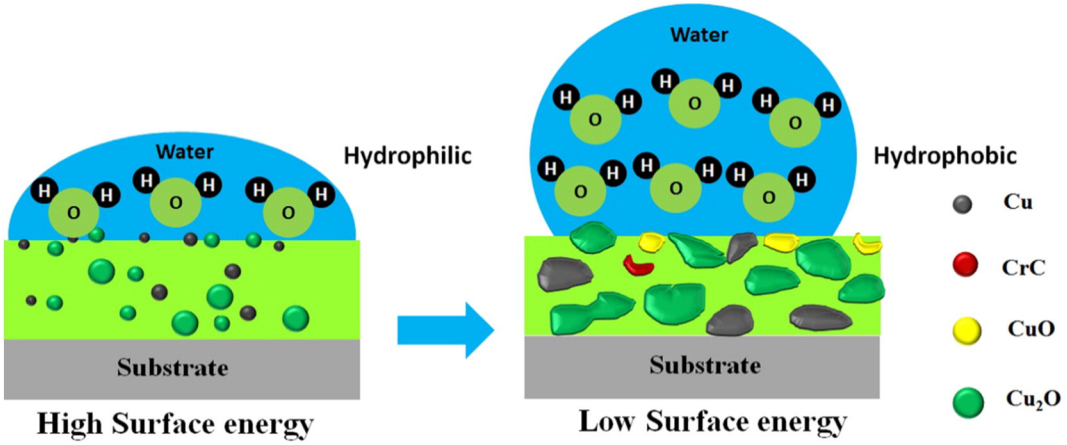

Fig. 13. Evolution schematic of the wettability state of Cu/Cr-DLC films.

significant relaxation of distorted C—C bond length, meanwhile, the formation of Cr—C nanoparticles enhanced the hardness of films. Depending on the synergistic effect of Cu and Cr metals, we concluded that the polar component of the surface energy could be the deciding factor in the wetting of Cu/Cr-DLC films. Besides, the film topographical microstructure, especially when the R_{max} is in a certain range, has a galvanizing impact on the hydrophobicity of films. Most importantly, our result provides a straightforward and facile method by using the synergistic benefits from the co-doped metal feature to manipulate the new nano-composite carbon-based films with good hydrophobicity and excellent mechanical performance for the promising applications in harsh marine environments.

Prime novelty statement

We firstly fabricated Cu and Cr co-doped diamond-like carbon (Cu/Cr-DLC) films using a facile hybrid ion beam deposition system. The resultant Cu/Cr-DLC films showed good hydrophobicity and superior mechanical performance with a relatively high water contact angle of 103.6°, lower residual stress of 0.89 GPa and high hardness of 13.44 GPa.

Acknowledgments

This work was financially supported by the National Natural Science Foundation of China (51522106, 51402319), State Key Project of Fundamental Research of China (2012CB933003, 2013CB632302) and International Science & Technology Cooperation Program of China (2014DFG52430).

References

[1] Y. Zhou, B. Wang, X. Song, E. Li, G. Li, S. Zhao, et al., Control over the wettability of amorphous carbon films in a large range from hydrophilicity to super-hydrophobicity, Appl. Surf. Sci. 253 (5) (2006) 2690–2694.
[2] D. Caschera, B. Cortese, A. Mezzi, M. Brucale, G.M. Ingo, G. Gigli, et al., Ultra hydrophobic/superhydrophilic modified cotton textiles through functionalized diamond-like carbon coatings for self-cleaning applications, Langmuir 29 (8) (2013) 2775–2783.
[3] K. Park, H.J. Choi, C. Chang, R.E. Cohen, G.H. McKinley, G. Barbastathis, Nanotextured silica surfaces with robust superhydrophobicity and omnidirectional broadband supertransmissivity, ACS Nano 6 (5) (2012) 3789–3799.
[4] X. Zhang, F. Shi, J. Niu, Y. Jiang, Z. Wang, Superhydrophobic surfaces: from structural control to functional application, J. Mater. Chem. 18 (6) (2008) 621–633.
[5] L. Feng, S. Li, Y. Li, H. Li, L. Zhang, J. Zhai, et al., Super-hydrophobic surfaces: from natural to artificial, Adv. Mater. 14 (24) (2002) 1857–1860.
[6] R. Truesdell, A. Mammoli, P. Vorobieff, F. van Swol, C.J. Brinker, Drag reduction on a patterned superhydrophobic surface, Phys. Rev. Lett. 97 (4) (2006) 044504-1–044504-4.
[7] Y. Zhang, Y. Chen, L. Shi, J. Li, Z. Guo, Recent progress of double-structural and functional materials with special wettability, J. Mater. Chem. 22 (3) (2012) 799–815.
[8] P. Ragesh, V.A. Ganesh, S.V. Naira, A.S. Nair, A review on 'self-cleaning and multifunctional materials', J. Mater. Chem. A 2 (36) (2014) 14773–14797.
[9] X. Du, X. Huang, X. Li, X. Meng, L. Yao, J. He, et al., Wettability behavior of special microscale ZnO nail-coated mesh films for oil-water separation, J. Colloid Interface Sci. 458 (2015) 79–86.
[10] S. Lee, W. Kim, S. Lee, S. Shim, D. Choi, Controlled transparency and wettability of large-area nanoporous anodized alumina on glass, Scr. Mater. 104 (2015) 29–32.
[11] J. Robertson, Diamond-like amorphous carbon, Mater. Sci. Eng. R 37 (4–6) (2002) 129–281.
[12] A.H. Lettington, Applications of diamond-like carbon thin films, Carbon 36 (5–6) (1998) 555–560.
[13] J. Brand, R. Gadow, A. Killinger, Application of diamond-like carbon coatings on steel tools in the production of precision glass components, Surf. Coat. Technol. 180-181 (2004) 213–217.
[14] C. Casiraghi, J. Robertson, A. Ferrari, Diamond-like carbon for data and beer storage, Mater. Today 10 (1–2) (2007) 44–53.
[15] Q. Wang, H. Yu, L. Zhong, J. Liu, J. Sun, J. Shen, Incorporation of silver ions into ultrathin titanium phosphate films: in situ reduction to prepare silver nanoparticles and their antibacterial activity, Chem. Mater. 18 (7) (2006) 1988–1994.
[16] F. Marciano, L. Bonetti, L. Santos, N. Da-Silva, E. Corat, V. Trava-Airoldi, Antibacterial activity of DLC and Ag-DLC films produced by PECVD technique, Diam. Relat. Mater. 18 (5–8) (2009) 1010–1014.
[17] P. Zhang, B. Tay, G. Yu, S. Lau, Y. Fu, Surface energy of metal containing amorphous carbon films deposited by filtered cathodic vacuum arc, Diam. Relat. Mater. 13 (3) (2004) 459–464.
[18] J. Chen, S. Lau, Z. Sun, G. Chen, Y. Li, B. Tay, et al., Metal-containing amorphous carbon films for hydrophobic application, Thin Solid Films 398-399 (2001) 110–115.
[19] P. Guo, L. Sun, X. Li, S. Xu, P. Ke, A. Wang, Structural properties and surface wettability of Cu-containing diamond-like carbon films by a hybrid linear ion beam deposition technique, Thin Solid Films 584 (2015) 289–293.
[20] W. Dai, H. Zheng, G. Wu, A. Wang, Effect of bias voltage on growth property of Cr-DLC film prepared by linear ion beam deposition technique, Vacuum 85 (2) (2010) 231–235.
[21] L. Ostrovskaya, V. Perevertailo, L. Matveeva, P. Milani, V. Ralchenko, E. Shpilevsky, Characterization of different carbon nanomaterials promising for biomedical and sensor applications by the wetting method, Powder Metall. Met. Ceram. 42 (1–2) (2003) 1–8.
[22] X. Li, P. Guo, L. Sun, A. Wang, P. Ke, Ab initio investigation on the novel Cu/Cr co-doped amorphous carbon nanocomposite films with giant residual stress reduction, ACS Appl. Mater. Interfaces 7 (2015) 27878–27884.
[23] F. Fowkes, Attractive forces at interfaces, Ind. Eng. Chem. 56 (12) (1964) 40–52.
[24] D.K. Owens, R.C. Wendt, Estimation of the surface free energy of polymers, J. Appl. Polym. Sci. 13 (8) (1969) 1741–1747.
[25] M.H. Ahmed, J.A. Byrne, J. McLaughlin, Kinetics and thermodynamics of human serum albumin adsorption on silicon doped diamond like carbon, Mater. Chem. Phys. 154 (2015) 84–93.
[26] D. Banerjee, S. Mukherjee, K. Chattopadhyay, Controlling the surface topology and hence the hydrophobicity of amorphous carbon thin films, Carbon 48 (4) (2010) 1025–1031.
[27] D. Depla, On the effective sputter yield during magnetron sputter deposition, Nucl. Instrum. Methods. B 328 (2014) 65–69.
[28] A. Ferrari, J. Robertson, Interpretation of Raman spectra of disordered and amorphous carbon, Phys. Rev. B 61 (20) (2000) 14095–14107.
[29] W. Dai, P. Ke, A. Wang, Microstructure and property evolution of Cr-DLC films with different Cr content deposited by a hybrid beam technique, Vacuum 85 (8) (2011) 792–797.
[30] L. Yate, L. Martínez-de-Olcoz, J. Esteve, A. Lousa, Effect of the bias voltage on the structure of nc-CrC/a-C: H coatings with high carbon content, Surf. Coat. Technol. 206 (11 − 12) (2012) 2877–2883.
[31] M. Huang, J. Jao, C. Lin, W. Hsieh, Y. Yang, L. Cheng, et al., Cathodoluminescence of Cr-doped diamond-like carbon film by filtered cathodic vacuum arc plasma, Appl. Surf. Sci. 261 (2012) 21–24.
[32] I. Nakai, Y. Sugitani, K. Nagashima, Y. Niwa, X-ray photoelectron spectroscopic study of copper minerals, J. Inorg. Nucl. Chem. 40 (5) (1978) 789–791.
[33] I. Jirka, An ESCA study of copper clusters on carbon, Surf. Sci. 232 (3) (1990) 307–315.
[34] J. Ghijsen, L. Tjeng, J. Vanelp, H. Eskes, J. Westerink, G. Sawatzky, et al., Electronic structure of Cu_2O and CuO, Phys. Rev. B 38 (16) (1988) 11322–11330.
[35] P.E. Hovsepian, Y.N. Kok, A.P. Ehiasarian, R. Haasch, J.G. Wen, I. Petrov, Phase separation and formation of the self-organised layered nanostructure in C/Cr coatings in conditions of high ion irradiation, Surf. Coat. Technol. 200 (5–6) (2005) 1572–1579.
[36] P. Hovsepian, Y. Kok, A. Ehiasarian, A. Erdemir, J. Wen, I. Petrov, Structure and tribological behaviour of nanoscale multilayer C/Cr coatings deposited by the combined steered cathodic arc/unbalanced magnetron sputtering technique, Thin Solid Films 447 (2004) 7–13.
[37] B. Balamurugan, B. Mehta, S. Shivaprasad, Surface-modified CuO layer in size-stabilized single-phase Cu_2O nanoparticles, Appl. Phys. Lett. 79 (19) (2001) 3176–3178.
[38] N. Dwivedi, S. Kumar, H.K. Malik, C. Sreekumar, S. Dayal, C.M.S. Rauthan, et al., Investigation of properties of Cu containing DLC films produced by PECVD process, J. Phys. Chem. Solids 73 (2) (2012) 308–316.
[39] W. Dai, G. Wu, A. Wang, Preparation, characterization and properties of Cr-incorporated DLC films on magnesium alloy, Diam. Relat. Mater. 19 (10) (2010) 1307–1315.
[40] C. Zou, H. Wang, L. Feng, S. Xue, Effects of Cr concentrations on the microstructure, hardness, and temperature-dependent tribological properties of Cr-DLC coatings, Appl. Surf. Sci. 286 (2013) 137–141.
[41] R.K. Roy, H. Choi, S. Park, K. Lee, Surface energy of the plasma treated Si incorporated diamond-like carbon films, Diam. Relat. Mater. 16 (9) (2007) 1732–1738.
[42] L. Ostrovskaya, A. Dementiev, I. Kulakova, V. Ralchenko, Chemical state and wettability of ion-irradiated diamond surfaces, Diam. Relat. Mater. 14 (3–7) (2005) 486–490.
[43] L. Ostrovskaya, Studies of diamond and diamond-like film surfaces using XAES, AFM and wetting, Vacuum 68 (3) (2002) 219–238.
[44] A.M. Asl, P. Kameli, M. Ranjbar, H. Salamati, M. Jannesari, Correlations between microstructure and hydrophobicity properties of pulsed laser deposited diamond-like carbon films, Superlattice. Microst. 81 (2015) 64–79.
[45] C.I. Pearce, R.A.D. Pattrick, D.J. Vaughan, C.M.B. Henderson, G. van der Laan, Copper oxidation state in chalcopyrite: mixed Cu d^9 and d^{10} characteristics, Geochim. Cosmochim. Acta 70 (18) (2006) 4635–4642.
[46] B. Zhang, S. Liu, W. Xu, Y. Cheng, Controllable wettability and morphology of electrodeposited surfaces on zinc substrates, Appl. Surf. Sci. 360 (2016) 904–914.